

pubs.acs.org/cm Article

A Structure—Activity Study of Aromatic Acid Modulators for the Synthesis of Zirconium-Based Metal—Organic Frameworks

Faith E. Chen,[‡] Tristan A. Pitt,[‡] Diane J. Okong'o, Luc G. Wetherbee, José J. Fuentes-Rivera, and Phillip J. Milner*



Cite This: Chem. Mater. 2022, 34, 3383-3394



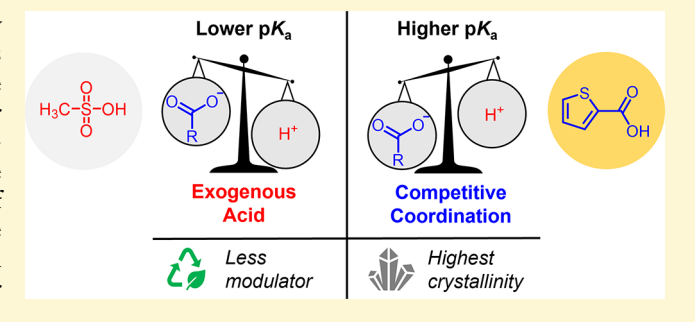
ACCESS I

III Metrics & More

Article Recommendations

SI Supporting Information

ABSTRACT: Acid modulation is among the most widely employed methods for preparing metal—organic frameworks (MOFs) that are both stable and highly crystalline, yet there exist few guiding principles for selecting the optimal modulator for a given system. Using the Zr-based MOFs UiO-66 and UiO-68-Me₂ (UiO = Universitetet i Oslo) as representative materials, here we present for the first time an in-depth structure—activity study of acid modulators and identify key principles of modulation for the synthesis of highly crystalline Zr-MOFs. By applying whole pattern fitting of powder X-ray diffraction patterns as a technique for evaluating modulator efficacy, complemented by scanning electron



microscopy, 1H NMR, and thermogravimetric analysis (TGA), we demonstrate that the key to effective modulation is competition between the linker and modulator for coordination to the Zr secondary building units (SBUs). Specifically, we illustrate that a close match in pK_a and structure between the linker and modulator favors larger and more well-defined crystallites, particularly with sterically unhindered aromatic acid modulators. Based on our findings, we demonstrate that 5-membered heteroaromatic carboxylic acids are among the most efficient acid modulators identified to date for the synthesis of several representative Zr-MOFs with **fcu** net topologies. In addition, we find that coordination modulation is superior to exogenous acid modulation at higher modulator concentrations. Finally, we compare 1H NMR and TGA as data-driven methods for quantifying linker deficiencies in modulated MOF syntheses. The guiding principles established herein have critical implications for the scalable and controllable synthesis of highly crystalline and stable MOFs relevant to chemical separations, gas storage, and catalysis.

■ INTRODUCTION

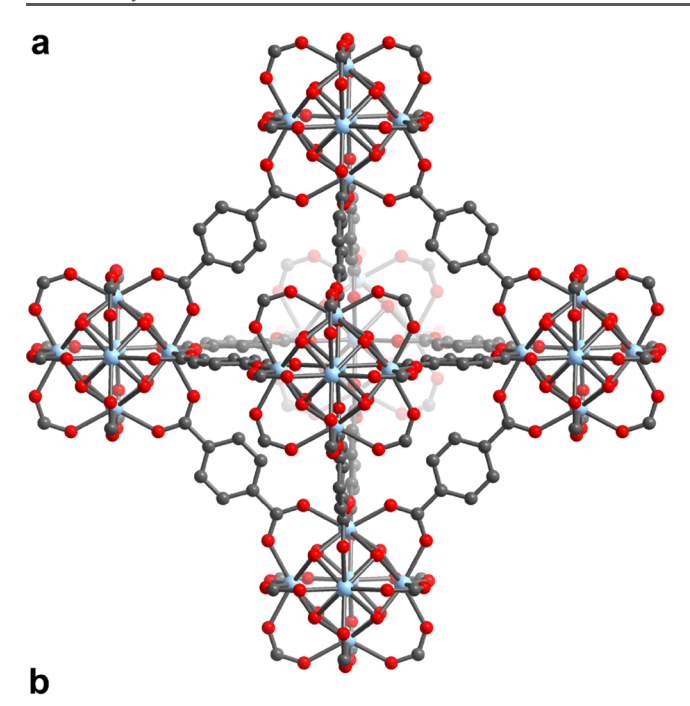
Metal-organic frameworks (MOFs) are porous, crystalline materials that have drawn widespread attention due to their potential applications in catalysis, separation, gas storage, and beyond. These materials self-assemble via the reversible coordination of polytopic organic linkers to inorganic secondary building units (SBUs). The reversibility of this interaction is the key to achieving high crystallinity. By varying the metal and/or linker, one can access a wide range of MOF topologies, reactivities, or stabilities, leading to an unparalleled degree of structural tunability among porous solids. Zirconiumbased frameworks (Zr-MOFs), such as UiO-66 (UiO = Universitetet i Oslo; Figure 1a),² exhibit remarkable chemical robustness among MOFs, which makes them especially promising for harsh applications such as in drug delivery and organic synthesis.^{3,4} However, this stability is a double-edged sword: the Zr-O bonds holding these frameworks together are stronger than other common MOF linkages and therefore limit reversibility during MOF formation. As such, Zr-MOFs often possess modest crystallinity compared to other frameworks, limiting their utility and hindering their structural characterization.⁵ Reliable control over the average size of Zr-MOF crystallites could unlock the full potential of these frameworks in important applications not available to less robust materials.

Modulators, such as monocarboxylic acids, can be used to improve the crystallinity of Zr-MOFs by enhancing the reversibility of MOF formation. Two potential mechanisms of modulation can be envisioned (Figure 1b): (1) the conjugate acid of the modulator protonates the linker from the node, and (2) the conjugate base of the modulator competes with the linker for coordination to the node, resulting in missing-linker and/or missing-cluster defects. Recent *in situ* studies of Zr-MOF formation kinetics support the latter mechanism. Notably, modulation can be used to control crystallite size and defect distribution within MOFs, both of which significantly impact framework properties.

Received: January 24, 2022 Revised: March 15, 2022 Published: March 28, 2022







Mechanism 1: Exogenous Acid

Mechanism 2: Competitive Coordination

Figure 1. (a) Structure of UiO-66. Gray, red, and light blue spheres correspond to C, O, and Zr, respectively. H atoms are omitted for clarity. (b) Mechanisms for the modulation of UiO-66 and other Zr-based MOF syntheses by exogenous acid or competitive coordination modulation.

In the first report of modulation of Zr-MOFs by carboxylic acids, Behrens and coworkers demonstrated that incorporating larger quantities of acid led to larger crystallites of MOFs in the UiO series. Osubsequently, a number of acid modulators have been investigated for Zr-MOF modulation, including formic acid, cacid, acetic acid, trifluoroacetic acid, dichloroacetic acid, dichloroacetic acid, and benzoic acid, among others. Overall, these studies indicate that lower p K_a and higher quantities of modulator generally favor increased crystallite sizes and defect incorporation. Nevertheless, MOF syntheses are frequently not optimized with regard to the identity and amount of modulator

used, often resulting in the addition of large quantities of modulator to produce highly crystalline frameworks. ^{27,28} When optimization of modulating conditions is attempted, it is usually done so by trial-and-error, hindering the discovery of new materials. Importantly, a better understanding of the relationship between the acid/conjugate base structure and modulating ability could enable rational and precise control over MOF crystallite size with a minimal amount of modulator.

Despite several acids having already been tested as modulators in Zr-MOF syntheses, a complete structureactivity study of acid modulators remains lacking. Herein, we systematically evaluate over 20 acid modulators for the synthesis of UiO-66 in order to determine which structural features govern modulation behavior, focusing specifically on pK_a and the structure of the conjugate base as critical factors. The efficacy of modulation is evaluated on the basis of volumeweighted average crystalline domain sizes—quantified by refining powder X-ray diffraction (PXRD) patterns—and by scanning electron microscopy (SEM). Additionally, ¹H NMR and thermogravimetric analysis (TGA) data are directly compared as methods for quantifying linker deficiencies and thus defects in modulated UiO-66 syntheses. Ultimately, the results presented herein suggest that pK_a is the most significant consideration at low modulator concentrations, but at higher modulator concentrations, aromatic carboxylic acids are the best candidates to produce large, well-defined crystallites. This is due to the close structural match of their aromatic conjugate bases with the aromatic linker. Among aromatic acids, steric effects significantly influence modulating ability, with more hindered modulators producing smaller average crystalline domain sizes. Based on this finding, we demonstrate that 5membered heteroaromatic carboxylic acids are among the best acid modulators identified to date for the synthesis of several representative Zr-MOFs with fcu net topologies. The immediate results of this study provide unparalleled insights into the effect of an acid modulator structure on modulating performance in Zr-MOF syntheses. In doing so, this work lays an important foundation for identifying new, efficient modulators for the controlled synthesis of stable MOFs.

■ RESULTS AND DISCUSSION

Evaluating Acid Modulators. Prior studies into modulated MOF syntheses have studied modulator efficacy using informative but relatively low-throughput techniques such as small-angle neutron scattering (SANS),²⁹ energy-dispersive X-ray diffraction (EDXRD),¹³ and transmission electron microscopy (TEM).^{14,29–32} Other studies have utilized more widely accessible methods such as static and dynamic light scattering (DLS)^{10,31,33} and turbidity measurements.³⁴ However, the latter techniques relate the efficacy of modulation to sizes of particles formed or to hydrodynamic radii and thus cannot reliably distinguish between aggregates of amorphous/ poorly crystalline materials and individual crystallites. In addition to these methods, SEM has been used previously to evaluate apparent crystallite sizes in studies of acid modulation, 10,13,14,30-32,34 but it is most useful only when the individual crystallites are relatively large and well defined. Critically, SEM only reveals particle size, not crystallite size, and so while it may reveal apparent, well-defined crystallites, it cannot confirm the formation of large crystalline domains without supplemental X-ray diffraction or more sophisticated electron microscopy techniques.

Due to the potential pitfalls with the aforementioned techniques, herein we employ whole powder pattern fitting as a complementary method for evaluating the efficacy of different acid modulators. Specifically, we quantify the volume-weighted average crystalline domain sizes (LVol-IB) of modulated UiO-66 samples by refinement of PXRD patterns using DIFFRAC.TOPAS V6 (Figure 2). Whole pattern fitting

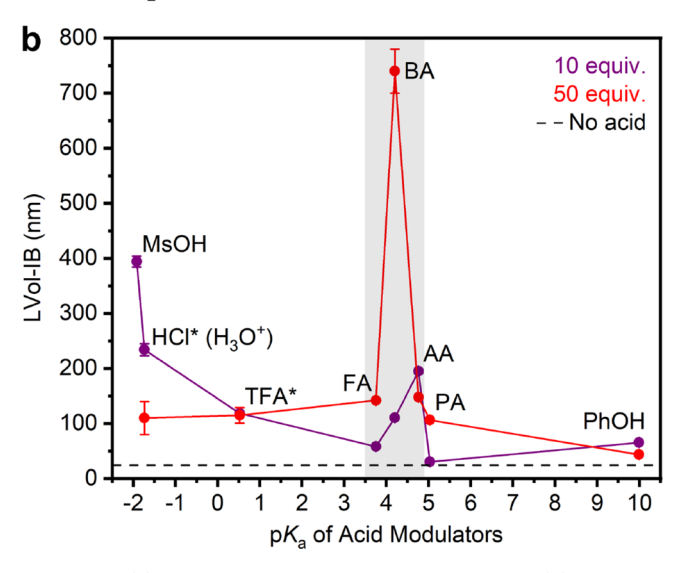


Figure 2. (a) Acid-modulated synthesis of UiO-66. (b) Volume-weighted average crystalline domain sizes (LVol-IB) vs modulator pK_a of UiO-66 samples prepared using 10 or 50 equiv of acid modulator. The gray box indicates the range between the pK_{a1} and pK_{a2} values of terephthalic acid. The star indicates modulators for which impurities were observed at 50 equiv. No MOF was formed when 50 equiv of MsOH was used. Note: some error bars are too small to see.

is a powerful quantitative method rooted in experimental X-ray diffraction, making it more dependable than other methods that may inaccurately equate crystallite size to other physical properties.³⁵ Notably, whole pattern fitting is distinct from the widely used practice of calculating full-width-at-half-maximum (FWHM) values of individual peaks in PXRD patterns to approximate the average crystallite sizes of MOFs using the Scherrer equation. 4,10,13,34,36 While both techniques can be used to obtain average crystalline domain sizes, whole powder pattern fitting is preferable to singling out specific peaks because the entire diffraction pattern is considered alongside microstructural features (such as strain) that influence peak profile shapes and positions.³⁷ Instrumental effects, peak asymmetries, and background signals are also better modeled using this approach. Importantly, integral breadth (IB) was chosen to quantify average crystalline domain size in our work rather than FWHM to reduce the effect of crystallite size distribution on the Scherrer constant (K). Critically, a close agreement between calculated average crystalline domain sizes and apparent crystallite sizes measured in SEM images of several UiO-66 samples supports our use of this method (Table S2). By contrast, Scherrer analysis of these same samples resulted in severely underestimated crystallite sizes

(Table S2 and Figure S3). Although we find close agreement between LVol-IB values and SEM images, we cannot rule out the possibility of amorphous domains in MOF samples.

All syntheses were carried out using a 1:1 ratio of terephthalic acid (H2bdc) and ZrCl4 in N,N-dimethylformamide (DMF) at 120 °C for 72 h, with 3 equiv of water added to facilitate Zr_6 cluster formation. The effect of modulator p K_8 on the average crystalline domain sizes of UiO-66 samples was initially assessed by modulating MOF syntheses under a standard set of conditions with 10 or 50 equiv of acids spanning a broad range of pK_a values (see the Supporting Information or Section 6 for details). The resulting samples were compared to a sample prepared without any added modulator, which possesses an average crystalline domain size of 24.3 \pm 0.5 nm (Figure 2a). Selected acids included those that have been previously studied, including concentrated hydrochloric acid (HCl),²⁰ trifluoroacetic acid (TFA),¹⁵ formic acid (FA),¹⁵ acetic acid (AA),^{10,15} and benzoic acid (BA), 10,26 as well as those that have not been studied to date, including methanesulfonic acid (MsOH), pivalic acid (PA), phenol (PhOH), and benzenesulfonamide (PhSO₂NH₂). In particular, non-carboxylic acid modulators such as MsOH (pK₂) = -1.92) and PhOH (p K_a = 10) were included to significantly broaden the pK_a range investigated compared to all previous studies. 9,15-24 After isolation, as-synthesized frameworks were extensively soaked in DMF and tetrahydrofuran (THF) to remove the residual starting material and modulator prior to characterization by powder X-ray diffraction (PXRD) and scanning electron microscopy (SEM). For simplicity, we refer to samples herein as UiO-66-mod-equiv, where mod is the modulator employed and equiv is the number of equivalents of modulator relative to ZrCl₄ and H₂bdc.

In syntheses employing 10 equiv of modulator, HCl and MsOH produced UiO-66 with the largest average crystalline domain sizes (Figure 2b), with the addition of stronger acids like concentrated sulfuric acid (H₂SO₄) completely inhibiting MOF formation. Notably, the strongest organic acid employed in this work, MsOH, forms the largest average crystalline domains of UiO-66 among all syntheses involving 10 equiv of modulator, with a calculated LVol-IB of nearly 400 nm. In addition, SEM images of UiO-66-MsOH-10 (Figure 3, SI Figure S29) show aggregates of large octahedra that, although incomplete, exhibit well-defined edges that are distinct from samples with smaller crystalline domains, such as those prepared with the same amount of formic acid (Figure S44).

The efficacy of MsOH as a modulator suggests that the exogenous acid mechanism dominates at low modulator concentrations. Indeed, the observed increase in average crystalline domain sizes from TFA to HCl (H_3O^+) to MsOH matches the corresponding decrease in pK_a in this series. This trend results from the ready dissociation of stronger acids to supply protons that protonate linker molecules and slow self-assembly of the framework.⁶ In addition, these stronger acids possess weakly nucleophilic conjugate bases that are unlikely to compete significantly with terephthalate for coordination to the SBU. Notably, MsOH enables the synthesis of UiO-66 with large crystalline domains at relatively low modulator concentrations compared to standard modulators,^{6,11,26} thereby providing a more efficient synthesis of this material.

Raising the modulator pK_a above -1.92 leads to smaller average crystalline domains until $pK_a = 3.75$ (FA), where a second spike in the average crystalline domain size is observed (Figure 2b). In this region, acid modulators with pK_a values

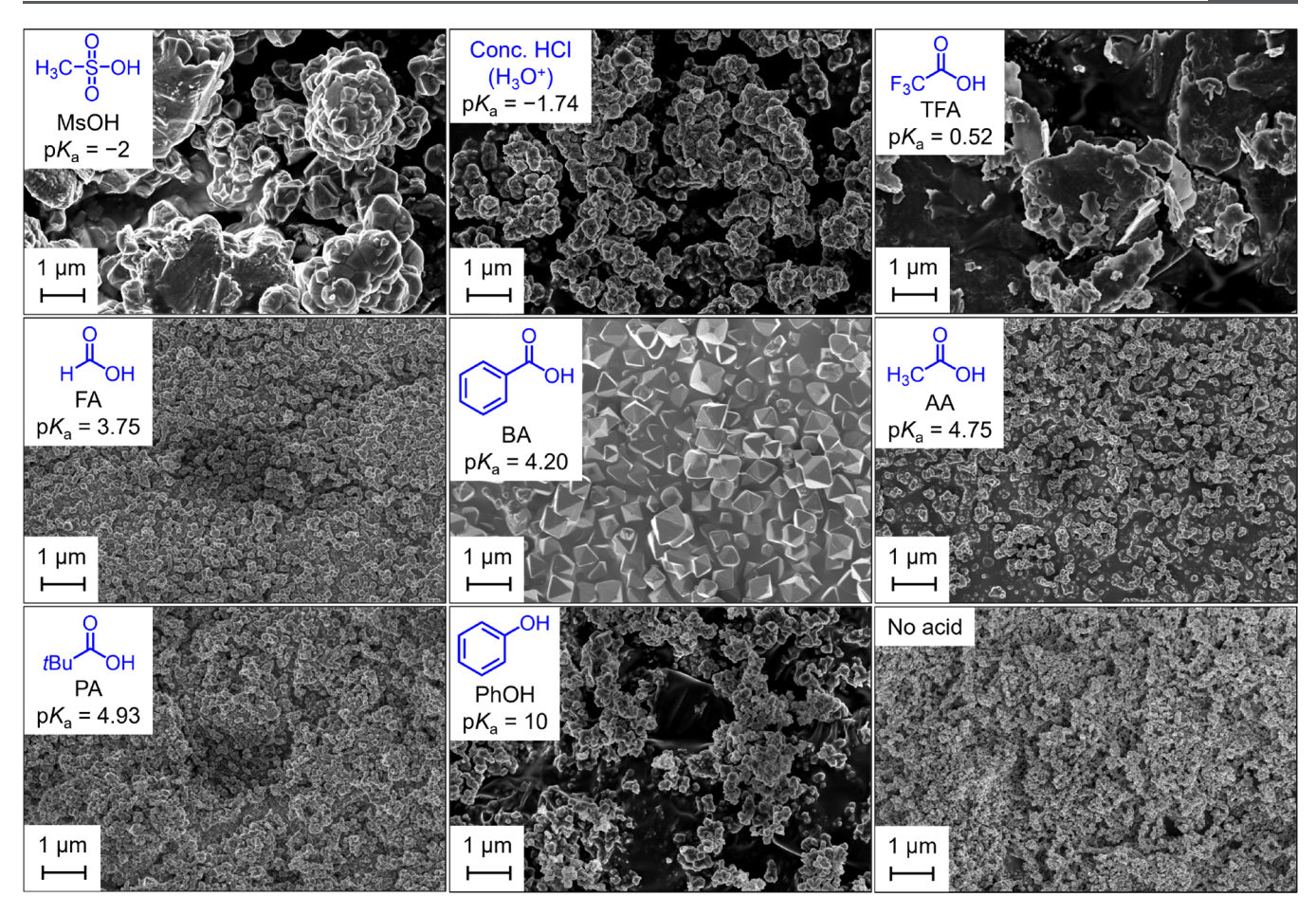


Figure 3. SEM images of UiO-66 samples prepared using 50 equiv of acid modulators. An image for UiO-66 prepared using 10 equiv of MsOH is included because no MOF was formed under these conditions using 50 equiv of modulator.

within the range of the first and second carboxylic acid protons of terephthalic acid (3.51 and 4.82, respectively) increase the average crystalline domain size relative to modulators with pK_a values outside of this range. As such, samples prepared with benzoic acid (pK_a = 4.20) and acetic acid (pK_a = 4.76) exhibit larger crystalline domains compared to those prepared with formic acid, which possesses a pK_a value near the lower limit of this range. Above the second pK_a of terephthalic acid, the average crystalline domain sizes of modulated UiO-66 samples drop precipitously. Indeed, modulation with PA (pK_a = 5.03), PhOH (pK_a = 10.0), or PhSO₂NH₂ (pK_a = 10.1, not shown) results in samples of similar crystalline domain sizes as unmodulated UiO-66.

We attribute this second spike in average crystalline domain size within the pK_a range of terephthalic acid to coordination modulation. This mechanism dominates when the nucleophilicities of the linker and conjugate base of the modulator are similar. In this case, both species can contend for coordination to Zr, slowing self-assembly of the MOF. By matching the nucleophilicity of terephthalic acid, benzoate and acetate effectively compete with the linker, resulting in the observed increase in average crystalline domain size when these modulators are used. Importantly, experiments demonstrating the successful modulation of UiO-66 with sodium trifluoroacetate (the use of which precludes exogenous acid modulation) support our hypothesis that competitive binding of the modulator's conjugate base is a viable modulation mechanism (see Section 10 for details). To the best of our

knowledge, this is the first demonstration that carboxylate salts can be employed as modulators in place of carboxylic acids. Unfortunately, the poor solubility of most other carboxylate salts in DMF precludes further study of this phenomenon.

Since increasing the amount of acid modulator is a widely employed method to improve the crystallite sizes of MOFs, we evaluated the effect of pK_a at higher concentrations by testing the same modulators at 50 equiv relative to ZrCl₄ and H₂bdc (Figures 2b and 3). The use of strong acids under these conditions led to the concomitant formation of insoluble impurities or inhibited MOF formation entirely, severely limiting the scope of exogenous acid modulation at higher acid concentrations. Indeed, the most effective modulator at 10 equiv, MsOH, inhibited MOF formation entirely at 50 equiv, likely due to its strong acidity. Meanwhile, impurities were identified in UiO-66 samples prepared using 50 equiv of TFA and HCl, which is consistent with previous findings. 15,20 In addition to the reo phase that is a consequence of ordered missing cluster defects $(2\theta = 4^{\circ})^{38}$ an additional impurity was observed at $2\theta = 7.0^{\circ}$ in UiO-66-HCl-50 (Figure S18).²⁰ Likewise, UiO-66-TFA-50 contained the reo phase in addition to numerous peaks that are attributed to unknown impurities (Figure S39). 15 The crystalline domain sizes of UiO-66-TFA-50 and UiO-66-HCl-50 were also lower than in samples prepared using fewer equivalents of these acids. Lastly, the SEM images of these samples do not display the well-defined octahedra expected for effectively modulated samples of UiO-66 (Figure 3).¹⁰ These results suggest that strong acids are

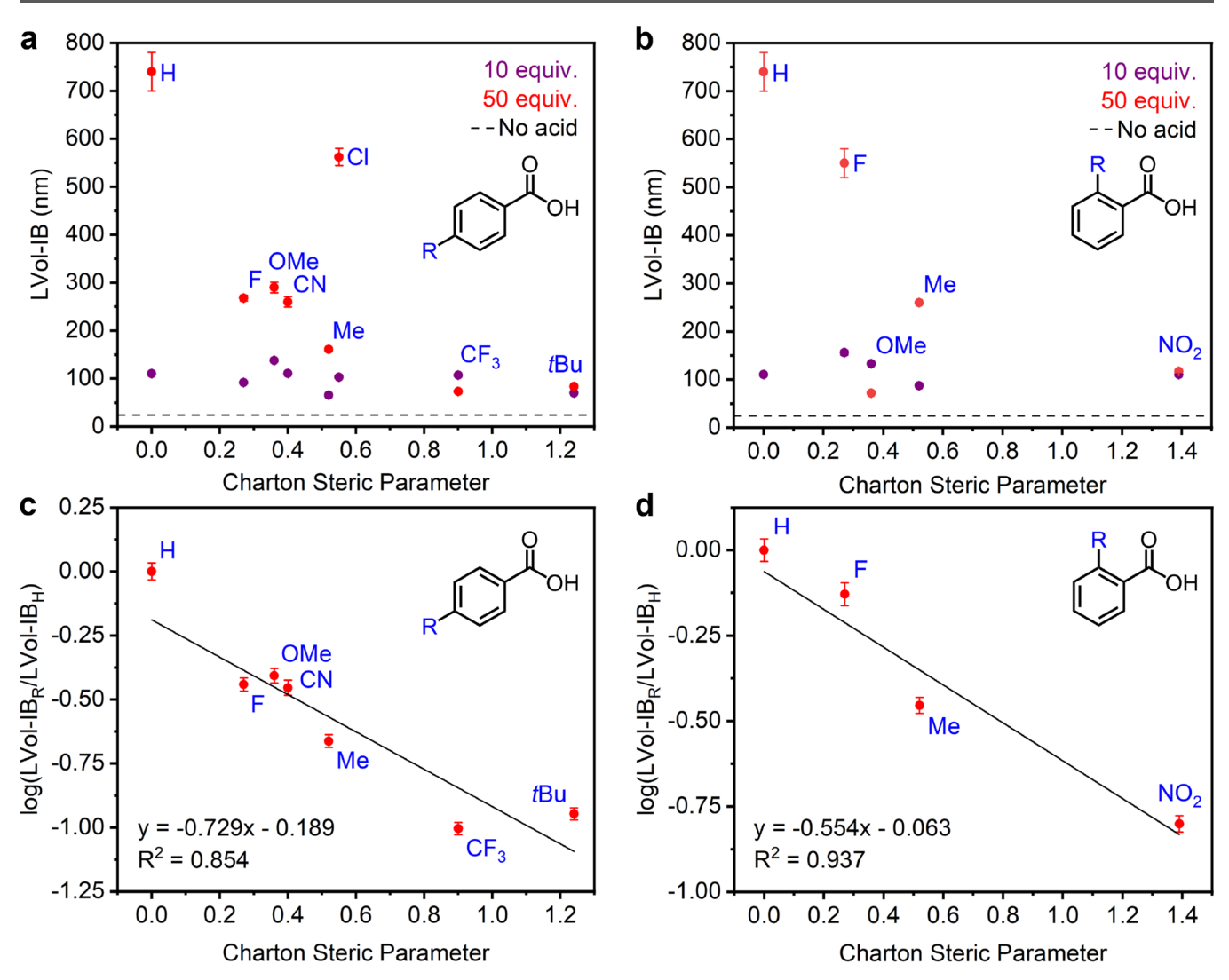


Figure 4. Volume-weighted average crystalline domain sizes (LVol-IB) vs Charton steric parameters of UiO-66 samples prepared using (a) parasubstituted and (b) ortho-substituted benzoic acid modulators. $Log(LVol-IB_R/LVol-IB_H)$ vs Charton steric parameters of UiO-66 samples prepared using (c) para-substituted and (d) ortho-substituted benzoic acid modulators. $LVol-IB_R$ and $LVol-IB_H$ refer to the average crystalline domain sizes of UiO-66 samples prepared using para- and ortho-substituted benzoic acid derivatives (R, identified in blue) and benzoic acid, respectively. UiO-66 prepared using 4-(methoxycarbonyl)benzoic acid was excluded from this analysis because the acid hydrolyzed to form additional terephthalate under the reaction conditions, based on TGA analysis (see Section 5 for details). UiO-66 prepared using 4-nitrobenzoic acid was excluded from this analysis because this acid completely suppressed MOF formation at 50 equiv of modulator. Samples prepared using ortho- and para-substituted benzoic acids are plotted separately for clarity. Note: some error bars are too small to see.

most effective when employed at low concentrations relative to H_2 bdc and $ZrCl_4$.

Although modulation with strong acids is problematic at higher acid concentrations, coordination modulation excels under these conditions. Indeed, samples prepared using 50 equiv of modulators with pK_a values within the range of terephthalic acid—namely, FA and BA—possess larger average crystalline domain sizes compared to other acids under these conditions (Figure 2b). Notably, the lack of a significant change between the average crystalline domain sizes of UiO-66-AA-10 and UiO-66-AA-50 compared to their TFA, FA, and BA counterparts is consistent with the literature. 15,26 Moreover, the trend of increasing crystalline domain size with increasing modulator concentration is mirrored in the SEM images, in which UiO-66 samples modulated with FA, AA, and BA show the best-defined apparent crystallites as well (Figure 3), especially compared to samples prepared with only 10 equiv of these acids (Figures S44, S62, and S53, respectively).

Among these samples, UiO-66-BA-50 exhibits the largest and most well-defined apparent crystallites by SEM, with particle sizes approximately matching its calculated average crystalline domain size (740 \pm 40 nm) determined by PXRD. The unique efficacy of BA as a modulator is likely due to its structural similarity to the linker (both are aromatic), which enables the *in situ* formation of benzoate-capped clusters that compete effectively with MOF crystallization. ^{26,39,40} In particular, the aromatic body of BA likely enables it to engage in similar intermolecular interactions as the linker (*e.g.*, π – π interactions) during MOF formation, making it an optimal competitor for the Zr nodes. As such, these findings suggest that aromatic acid derivatives are the most effective modulators for increasing the crystallite size and uniformity of UiO-66.

Benzoic Acid Derivatives. To gain further insight into the unique efficacy of BA as a modulator, UiO-66 syntheses were carried out using a range of *ortho*- and *para*-substituted benzoic acid derivatives (Figure 4). As before, modulator efficacy was

assessed using the volume-weighted average crystalline domain sizes (LVol-IB) determined by PXRD in conjunction with SEM. Although substituted benzoic acids have been previously employed as Zr-MOF modulators in scattered studies, ⁴¹ a clear structure—activity study relating how substituent steric and electronic effects affect modulator performance remains lacking. Establishing such structure—activity trends could enable the identification of superior modulators, especially when considering the already impressive modulating ability of unsubstituted BA.

We set out to probe electronic effects on modulator performance by employing BA derivatives bearing a range of para substituents, including electron-donating (4-OMe, 4-tBu, 4-Me), electron-neutral (H, BA), and electron-withdrawing (4-F, 4-Cl, 4-CF₃, 4-CN) groups (Figure 4a, see Section 7 for details). To elucidate possible electronic effects, Hammett constants (σ) were assigned to samples based on the identity of their associated para-substituted modulators.⁴² With 10 equiv of modulator, no significant differences in average crystalline domain sizes were observed among the substituted modulators. These samples also displayed small LVol-IB values and a lack of well-defined octahedra in SEM images (see Section 7 for images). Increasing the para-substituted modulator concentration from 10 to 50 equiv relative to ZrCl₄ increased the average crystalline domain sizes in nearly every case. However, attempts to relate LVol-IB values of samples to σ values revealed no clear trend between modulating ability and the electronic nature of the para substituent (Figure S168). The p K_3 values of substituted benzoic acids do not correlate with the crystalline domain sizes of UiO-66 samples either (Figures S169 and S209).

Careful analysis of the data revealed that benzoic acid modulators bearing bulky substituents in the para position (e.g., 4-tBu, 4-CF₃) produced similar crystalline domain sizes as samples prepared without any modulator, implying that substituent size, not electronic nature, may be a determining factor in modulating ability. To elucidate the role of steric effects implied by the poor performance of modulators bearing large substituents, Charton and STERIMOL B₁ steric parameters were assigned to samples based on their parasubstituted modulators instead of σ values.^{42,43} Critically, plotting the crystalline domain sizes of modulated UiO-66 samples against Charton steric parameters revealed that modulating ability exponentially decreases as the steric bulk of the substituent on the modulator increases (Figure 4a). The same effect was observed using STERIMOL B₁ parameters as well (Figure S167). Indeed, a plot of log(LVol-IB_R/LVol-IB_H) vs Charton parameter for various R groups on the modulator revealed an approximately linear trend ($R^2 = 0.854$) when excluding 4-Cl as an outlier (see below), indicative of a potential linear free-energy relationship between substituent size and average crystalline domain size (Figure 4c).

To further study the potential impact of modulator steric hindrance on performance, the average crystalline domain sizes of *ortho*-substituted benzoic acid-modulated UiO-66 samples were also evaluated using BA derivatives bearing a range of *ortho* substituents (2-F, 2-OMe, 2-Me, 2-NO₂; see Section 8 for details). Similar to the results obtained for *para*-substituted modulators, with 50 equiv of the *ortho*-substituted modulators, the average crystalline domain sizes generally decrease as the size of the *ortho*-substituent increases (Figure 4b). In this case, a plot of $\log(\text{LVol-IB}_R/\text{LVol-IB}_H)$ vs Charton parameter also revealed an approximately linear trend ($R^2 = 0.937$) when 2-

OMe was excluded as an outlier (see below), reflecting a clear trend between *ortho*-substituent size and modulator efficacy (Figure 4d). This shared trend among *para*- and *ortho*-substituted benzoic acids was also confirmed by SEM. For example, SEM images of UiO-66-4-F-50 and UiO-66-2-F-50 show large, similarly sized octahedra with sharp edges (Figures S118 and S197, respectively), while SEM images of UiO-66-4-tBu-50 reveal small globular particles (Figure S100), consistent with the poor modulating ability of this bulky carboxylic acid. Notably, the sizes of apparent octahedral crystallites measured in images of multiple samples (*e.g.*, UiO-66-4-F-50, UiO-66-2-F-50, and UiO-66-2-Me-50) agree well with their calculated crystalline domain sizes, further supporting the advantage of whole pattern fitting to determine crystallite size and thus modulator efficacy.

Two exceptions to the trend of decreasing modulating ability with increasing steric hindrance were observed: UiO-66-4-Cl-50 and UiO-66-2-OMe-50. The use of 4-chlorobenzoic acid led to remarkably large crystalline domains despite the large Charton and STERIMOL B₁ steric descriptors of a Cl atom. This is likely due to the polarizability of Cl, which allows 4chlorobenzoic acid to fit in tight spaces in the MOF where substituted benzoic acids of a similar size but lower polarizability (e.g., 4-methylbenzoic acid) cannot. Indeed, previous studies have demonstrated the same effect in molecular systems and concluded that Charton parameters do not accurately reflect polarizability. 44,45 Meanwhile, employing 50 equiv of 2-methoxybenzoic acid produced a material with small crystalline domains despite the relatively small Charton and STERIMOL B₁ steric descriptors of a methoxy group. This result was not observed with 4methoxybenzoic acid, which is likely because ortho substituents on the modulator point more directly at the SBU than those in the para position. While a methoxy group is relatively small from the perspective of the carbon to which it is attached, it occupies a larger volume than any other ortho substituents studied herein. For example, the volume of a methoxy group (175 Å³) exceeds that of a methyl group (167 Å³), despite sharing similar steric descriptors. 46 As a result, it may exhibit a stronger steric effect at longer distances. We hypothesize that in the ortho position, the methoxy group likely collides with the node to which the adjacent carboxylate is bound, leading to significant steric interactions that disfavor modulator competition and make 2-methoxybenxoic acid a worse modulator than might otherwise be expected.

We attribute the inverse relationship between crystalline domain and modulator sizes to the small pores (~6 Å)⁴⁷ of UiO-66, which may inhibit the conjugate bases of more sterically hindered modulators from diffusing through MOF pores and accessing SBU sites. The presence of fewer conjugate base molecules available to SBU sites consequently favors terephthalate binding, which in turn, drives the reaction equilibrium toward rapid MOF formation and kinetically controlled products. Likewise, sterically hindered conjugate bases would be less effective competitors even when they do reach the SBU. As such, small aromatic acid modulators lead to larger crystallites because their sterically unencumbered conjugate bases can diffuse more readily through the pores of the MOF and compete with terephthalate molecules for coordination to Zr. Ultimately, the findings outlined in Figure 4 represent the first definitive evidence for steric effects being a key parameter underpinning effective coordination modulation.

5-Membered Heteroaromatic Acid Modulators. The findings presented thus far suggest that small aromatic acid modulators within the range of pK_{a1} and pK_{a2} of terephthalic acid should be the most effective modulators for the synthesis of UiO-66. Based on these criteria, we hypothesized that 5-membered heteroaromatic acids would be ideal modulators due to their similar pK_a values yet smaller size compared to 6-membered aromatic acids. As Consistently, the kinetic diameter of thiophene (4.6 Å) is smaller than that of benzene (5.8 Å). As such, UiO-66 syntheses were modulated with 2-thiophenecarboxylic acid (2-TP, $pK_a = 3.49$) and 3-thiophenecarboxylic acid (3-TP, $pK_a = 4.08$) (Figure 5, see Section 9 for details). Indeed, at both 10 and 50 equiv of modulator, 2-TP and 3-TP outperform BA by forming UiO-66

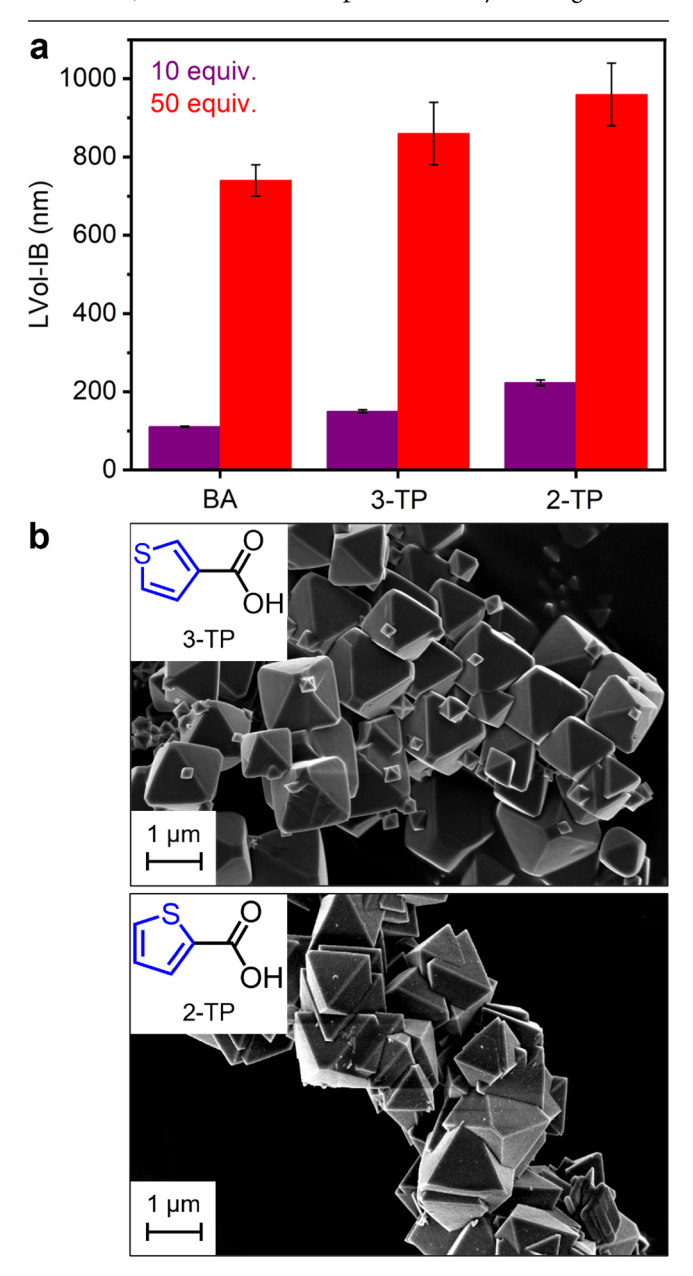


Figure 5. (a) Volume-weighted average crystalline domain sizes of UiO-66 samples prepared using 10 and 50 equiv of benzoic acid, 3-thiophenecarboxylic acid, and 2-thiophenecarboxylic acid. (b) SEM images of UiO-66 samples prepared using 50 equiv of 3-thiophenecarboxylic acid and 2-thiophenecarboxylic acid.

with larger average crystalline domains, as quantified by LVol-IB values (Figure 5a). Notably, 2-TP produced the largest UiO-66 crystallites among all modulators studied in this work, validating that pK_a and steric effects are the most critical factors governing modulator efficacy. We hypothesize that 2-TP outperforms 3-TP because it is more acidic and possesses only one H atom ortho to the carboxylic acid, whereas 3-TP possesses two. SEM images of both UiO-66-2-TP-50 and UiO-66-3-TP-50 reveal many apparent crystallites larger than 1 μ m in diameter (Figure 5b), surpassing the size of those prepared with BA, along with smaller apparent crystallites as well (Figure 3). The broader size distribution in UiO-66-2-TP-50 and UiO-66-3-TP-50 observed by SEM, relative to UiO-66-BA-50, likely accounts for the larger errors in the calculated average crystalline domain sizes of these samples. Overall, these findings suggest that 5-membered heteroaromatic acid modulators are a promising new platform for the synthesis of large and well-defined crystallites of UiO-66.

Defect Incorporation. In many cases, the use of carboxylic acid modulators in Zr-MOFs leads to their incorporation as substitution defects. The *in situ* hydrolysis of DMF under MOF-forming conditions introduces additional formate that can also coordinate to the SBU in place of the linker. To gain further insight into the nature of modulation in Zr-MOFs, we quantified the relative incorporations of the total modulator (modulator conjugate base + formate) in UiO-66 samples prepared in this work. Linker deficiencies, and thus modulator incorporation, can be quantified by ¹H NMR spectroscopy of acid-digested samples ^{15,17,21,26,50} and analysis of TGA decomposition profiles (see Section 5 for details). ^{10,12,20,38,47,51-55} The compiled results of both methods are available in the Supporting Information (Section 5).

Consistent with literature reports, ²⁶ NMR and TGA analyses of samples in this work show that the samples bearing the largest average crystalline domains of UiO-66 (LVol-IB > 200 nm) coalesce to 3-4 (out of a possible 6) terephthalate linkers per node, with the remaining sites capped by the modulator or formate as defects (Figure 6). The samples in this work that form the largest crystallites-namely, UiO-66-BA-50, UiO-66-2-TP-50, and UiO-66-3-TP-50—show approximately 44% total modulator incorporation, as quantified by ¹H NMR. Critically, we did not observe any samples that possess large crystalline domains and low amounts of modulator incorporated as defects (upper right section of Figure 6). In samples with smaller crystalline domains (empirically determined as LVol-IB <200 nm), the extent of linker incorporation generally skews toward a higher number of linkers incorporated compared to modulators (Figure 6 and Figures S4 and S5), possibly due to the weaker ability of their associated modulators to compete with terephthalate. Overall, these findings indicate that a high degree of defectiveness does not imply high crystallinity, but samples with large crystalline domain sizes do tend to possess a large degree of linker substitution defects due to coordinative displacement of the linker by the modulator.

While ¹H NMR and TGA have previously been used in tandem for missing-linker quantification on small numbers of samples, ^{15,24,25,34,56} they have not been thoroughly compared, especially with enough samples to analyze their respective efficacies. The quantity of UiO-66 samples of differing average crystalline domain sizes prepared in this work enables a thorough comparison of both data-driven approaches for quantifying linker deficiencies in modulated UiO-66 samples.

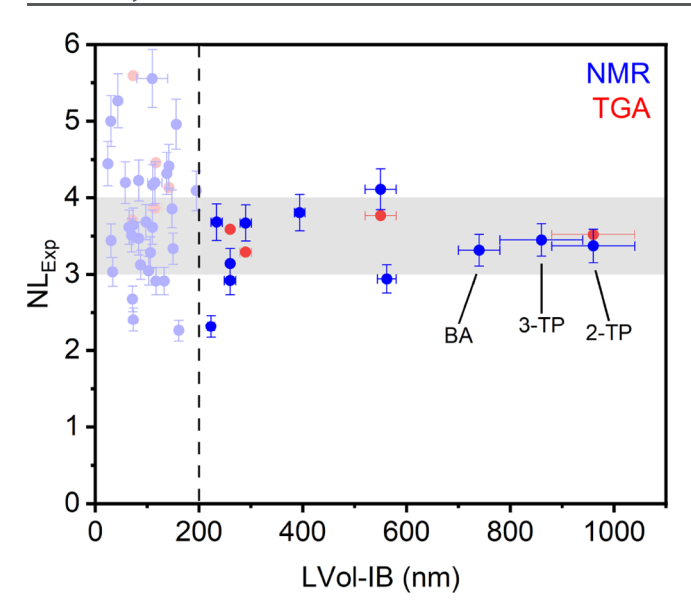


Figure 6. Number of linkers quantified by TGA and/or 1 H NMR spectroscopy (NL_{Exp}) vs volume-weighted average crystalline domain sizes of UiO-66 samples prepared using 10 and 50 equiv of acid modulators. The gray box indicates 33–50% incorporation of total modulators as defects (formate + modulator conjugate base). The three indicated samples were prepared using 50 equiv of modulator. Only TGA data in which dehydroxylated plateaus were apparent from the decomposition profiles are included (see Section 5 for details). Note: some error bars are too small to see.

Notably, the utility of TGA is hindered by the absence of clear dehydroxylated regimes in the decomposition profiles of many samples, which introduces considerable uncertainty into quantifying the experimental number of linkers by this method. Meanwhile, analysis of acid-digested MOFs by NMR is more consistently applicable but assumes that the total amount of modulator observed was once covalently bound to an SBU, which may not be true for large modulators such as orthosubstituted benzoic acid derivatives that can become trapped within the framework pores. Accordingly, samples such as UiO-66-2-OMe-50, UiO-66-4-CF₃-50, and UiO-66-4-Me-50 display an unrealistically high degree of linker deficiencies by NMR analysis due to the higher-than-expected presence of modulator within the structure. Generally, we find that the precision of linker deficiencies quantified by TGA and ¹H NMR is directly related to the average crystalline domain sizes of UiO-66 samples (Figures S6 and S7), underscoring the benefit of using both analyses before drawing conclusions.

Porosity. Missing linker and missing cluster defects that arise from modulator incorporation commonly cause UiO-66 samples to exhibit surface areas significantly larger than the theoretical maximum (\sim 1200 m²/g). ^{15,18,20} In particular, samples modulated by strong acids (e.g., TFA and HCl), including those in this work, often contain the reo phase due to ordered missing cluster defects, leading to high surface areas. 15,38 Motivated by the extent of defect incorporation in UiO-66-2-TP-50 and UiO-66-3-TP-50 and recognizing that smaller modulators occupy less space in the pores of MOFs than larger modulators, we investigated whether 5-membered heteroaromatic carboxylic acid-modulated MOFs exhibited enhanced surface areas compared to their BA-modulated analogues. To this end, large scale (LS) samples of UiO-66 using 2-TP, 3-TP, BA, and no acid modulator were prepared and analyzed by 77 K N₂ adsorption measurements (see

Section 11 for details). A sample of UiO-66 prepared using 5 equiv of MsOH, the best acid modulator at low concentrations, was also prepared for comparison. The average crystalline domain sizes of these samples were similar to those prepared on a small scale (Table S5). In all cases, the frameworks were found to be microporous, and the adsorption data could be fit to yield 77 K N₂ Brunauer–Emmett–Teller (BET) surface areas (Table 1). Importantly, the BET surface area of UiO-66

Table 1. Brunauer–Emmett–Teller (BET) Surface Areas of Large Scale (LS) UiO-66 Samples, as Determined from 77 K N₂ Adsorption Measurements

sample	BET surface area (m^2/g)
UiO-66-3-TP-50-LS	1778 ± 4
UiO-66-BA-50-LS	1718 ± 7
UiO-66-2-TP-50-LS	1565 ± 7
UiO-66-MsOH-5-LS	1231 ± 4
UiO-66-no acid-LS	1097 ± 6

modulated by 3-TP (1778 \pm 4 m²/g) exceeded that of UiO-66 prepared with BA (1718 \pm 7 m²/g) and is among the highest reported values for phase-pure (*i.e.*, lacking the **reo** phase) UiO-66 absent post-synthetic modifications. ^{f1,14,37} Meanwhile, the surface area of UiO-66 modulated with 2-TP is competitive with the sample modulated with BA. Overall, 5-membered heteroaromatic acids were found to be promising modulators, as their use afforded the largest crystallites and high surface areas of UiO-66 in this work. Notably, we did not observe the **reo** phase in any of these samples by PXRD (Figures \$239–243), suggesting that missing linker defects may be dominant with these modulators.

Extension to Other Zr-MOFs. Motivated by the success of 2-TP and 3-TP as modulators for the synthesis of UiO-66, we assessed their ability to modulate the syntheses of other Zr-MOFs. Unfortunately, the synthesis of UiO-67, 2,47 an isoreticularly expanded analog of UiO-66, was found to yield inconsistent results due to the poor solubility of the linker under the reaction conditions (Figure S258), which led us to exclude it from this fundamental study of acid modulation (see Section 13 for details). Nevertheless, BA, 3-TP, and 2-TP were consistently found to be excellent modulators for synthesizing well-defined crystallites of this framework (Table S8). In contrast to the linker for UiO-67, the precursor H2dmtpdc (2',5'-dimethyl-[1,1':4',1"-terphenyl]-4,4"-dicarboxylic acid) corresponding to the isoreticularly expanded framework UiO-68-Me₂ (Figure 7a)⁵⁷ was found to be fully soluble under the reaction conditions, and thus UiO-68-Me2 was chosen as a second framework to evaluate the generality of our findings. Gratifyingly, utilizing both modulators at 10 equiv during the synthesis of UiO-68-Me2 substantially improved the average crystalline domain sizes of the resultant frameworks relative to BA-modulated and unmodulated samples (Figure 7b,c, see Section 12 for details). MOF formation was not observed when using 30 and 50 equiv of these modulators, likely due to the reduced stability of UiO-68-Me₂ compared to UiO-66. Matching the trend observed for UiO-66, 2-TP outperformed 3-TP to form UiO-68-Me2 with an average crystalline domain size of 1080 ± 60 nm (Figure 7b). Likewise, syntheses using TFA, FA, and AA formed poorly modulated UiO-68-Me₂ samples bearing small crystalline domains, once again highlighting the importance of the modulator's structural similarity to the linker, in addition to its size, for effective modulation

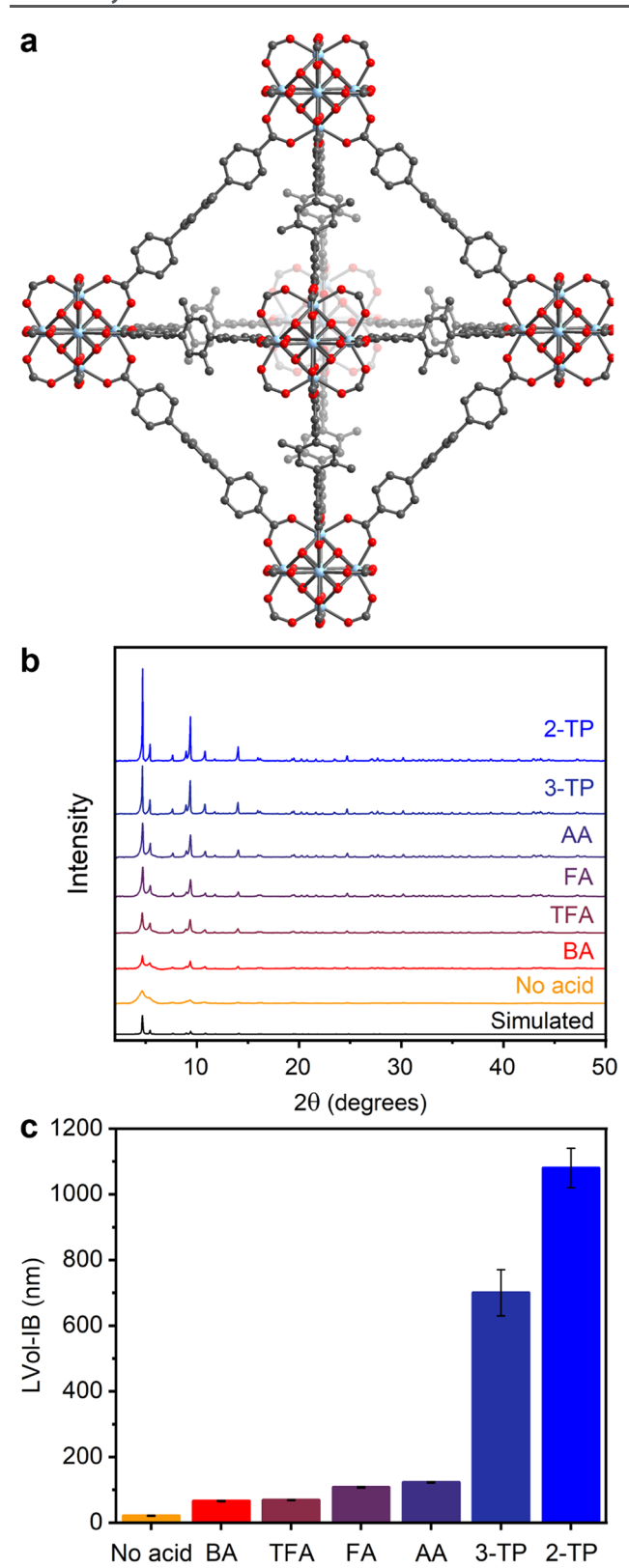


Figure 7. (a) Structure of UiO-68-Me₂. Gray, red, and light blue spheres correspond to C, O, and Zr, respectively. H atoms are omitted for clarity. (b) PXRD patterns of UiO-68-Me₂ samples prepared using 10 equiv of BA, TFA, FA, AA, 3-TP, 2-TP, and using no acid. The simulated pattern based on the single-crystal X-ray diffraction structure of UiO-68-Me₂ is included for reference. (c) Average crystalline domain sizes of UiO-68-Me₂ samples obtained by refining the corresponding PXRD patterns.

(Figure 7b). The reduced stability of UiO-68-Me₂ compared to UiO-66 likely makes it more sensitive to variations in the modulator structure than UiO-66, accounting for the drastic differences among modulators for this framework. Importantly, SEM images of UiO-68-Me₂ samples prepared in this work support the trends outlined by the PXRD data, with UiO-68-Me₂-2-TP-10 forming well-defined crystallites approximately 1 μ m in size (Figure S256, see Section 12 for images).

CONCLUSIONS

Acid modulation is one of the most widely employed methods for obtaining highly crystalline MOFs. Nevertheless, the optimal modulator for a given MOF synthesis is still largely determined by trial-and-error. The systematic structure—activity study of acid modulation in Zr-MOFs reported herein reveals several considerations for the synthesis of stable MOFs with large crystalline domains.

Our principal finding is that the key to optimal acid modulation, and subsequently the key to growing MOFs with large crystalline domains, is not just to add a strong acid but rather to add a strong competitor with the linker for coordination to the SBU. To be a strong competitor, the modulator should closely resemble the linker with regards to pK_a and structure (e.g., aromatic acid modulators for aromatic linkers) and should be as sterically unhindered as possible. At low concentrations of acid modulator, modulation by exogenous acid can be productive, as evidenced by syntheses using the strong organic acid MsOH. However, when employing acid modulators in the range of pK_{a1} and pK_{a2} of terephthalic acid, coordination modulation dominates and results in the largest average crystalline domains of UiO-66 samples prepared in this work. In addition, the use of substituted benzoic acid derivatives reveals that modulator size is a key parameter underpinning effective coordination modulation. The results of these structure-activity analyses reveal that benzoate forms large crystallites of UiO-66 because it meets the conditions to be an effective competitor with terephthalate for coordination to the SBU. Applying our criteria to identify even more productive modulators, we demonstrate that 5-membered heteroaromatic acids such as 3-TP and 2-TP surpass BA in modulation efficacy. Furthermore, their ability to modulate the synthesis of UiO-68-Me2 is an encouraging step toward demonstrating the generality of our criteria for effective modulation. In future work, we will broaden our focus to the syntheses of Zr-MOFs of different topologies (e.g., spn and csq nets), which commonly require multiple modulators, and extend our findings beyond Zr-MOFs to other families of frameworks.

■ EXPERIMENTAL SECTION/METHODS

General Procedures. Details are provided in the Supporting Information.

Example UiO-66 Synthesis. A screw-cap reaction tube was charged with terephthalic acid (12.5 mg, 0.075 mmol, 1.00 equiv) and ZrCl₄ (17.5 mg, 0.075 mmol, 1.00 equiv). If the modulator was a solid, it was added at this point. Next, deionized water (4.05 μ L, 0.225 mmol, 3.00 equiv), the modulator (if a liquid), and fresh DMF (1.5 mL) were added to the tube. The threads of the tube were wrapped in Teflon tape and the tube was capped. The tube was transferred to a stainless-steel block on a dry heating bath and the temperature was set to 120 °C. The tube was allowed to stand at 120 °C for 72 h. At this time, the tube was removed from the block and allowed to cool to room temperature. The supernatant was removed using a pipette, and fresh DMF (10 mL) was added. The tube was agitated and then

allowed to settle for 24 h. At this time, the supernatant was removed from the solid via a pipette, and fresh DMF (10 mL) was added. This soaking procedure was repeated for a total of three DMF soaks. The DMF was replaced with THF (10 mL), and the above procedure was repeated for a total of three THF soaks. The white solid was filtered, dried in air, and characterized by PXRD, NMR, SEM, and TGA. For samples that did not adequately settle after 24 h during the soaking process, the heterogeneous mixture was centrifuged at 4000 rpm for 15 min, and the solvent was decanted and replaced with fresh solvent. For samples that could not be filtered because they passed through a filter paper, the solvent after the final soak was removed under reduced pressure.

UiO-68-Me $_2$ and UiO-67 samples were prepared following a modified procedure in which H_2 (dmtpdc) (26.0 mg, 0.075 mmol, 1.00 equiv) or 4,4′-biphenyldicarboxylic acid (18.2 mg, 0.075 mmol, 1.00 equiv) was used in place of terephthalic acid and the DMF soaks were carried out at 60 $^{\circ}$ C instead of room temperature. The white solids were filtered, dried in air, and characterized by PXRD and SEM.

General Procedure for MOF Digestion. A 4 mL vial was charged with MOF (\sim 5 mg) and DMSO- d_6 (0.5 mL). Next, 2–5 drops of DCl (35 wt. % in D₂O) were added, and the vial was capped. The vial was heated at 100 °C in a heat block for 12 h until completely homogeneous. The solution was transferred to an NMR tube and analyzed by 1 H and 19 F NMR, where appropriate.

ASSOCIATED CONTENT

Supporting Information

The Supporting Information is available free of charge at https://pubs.acs.org/doi/10.1021/acs.chemmater.2c00241.

Experimental procedures, tabulated LVol-IB values, NMR data, TGA data, surface area data, as well as SEM images, PXRD patterns and refinements, NMR spectra, and TGA profiles of individual samples (PDF)

AUTHOR INFORMATION

Corresponding Author

Phillip J. Milner – Department of Chemistry and Chemical Biology, Cornell University, Ithaca, New York 14850, United States; orcid.org/0000-0002-2618-013X; Email: pjm347@cornell.edu

Authors

Faith E. Chen – Department of Chemistry and Chemical Biology, Cornell University, Ithaca, New York 14850, United States

Tristan A. Pitt – Department of Chemistry and Chemical Biology, Cornell University, Ithaca, New York 14850, United States

Diane J. Okong'o – Department of Chemistry and Chemical Biology, Cornell University, Ithaca, New York 14850, United States

Luc G. Wetherbee – Department of Chemistry and Chemical Biology, Cornell University, Ithaca, New York 14850, United States

José J. Fuentes-Rivera – Department of Chemistry and Chemical Biology, Cornell University, Ithaca, New York 14850, United States; oorcid.org/0000-0002-8861-6752

Complete contact information is available at: https://pubs.acs.org/10.1021/acs.chemmater.2c00241

Author Contributions

[‡]F.E.C. and T.A.P. contributed equally.

Funding

The development of scalable methods for the synthesis of MOFs was supported by the National Institute of General Medical Sciences of the National Institutes of Health under award number R35GM138165. The content is solely the responsibility of the authors and does not necessarily represent the official views of the National Institutes of Health. This work made use of the Cornell Center for Materials Research Shared Facilities, which are supported through the NSF MRSEC program (DMR-1719875). This work made use of a Bruker 500 MHz spectrometer, the purchase of which was supported by the National Science Foundation (CHE-1531632). We are grateful to Cornell University for providing Summer Experience Grants to F.E.C. and D.J.O.

Notes

The authors declare the following competing financial interest(s): P.J.M. is listed as a co-inventor on several patents related to the synthesis and applications of metal-organic frameworks.

ACKNOWLEDGMENTS

We thank Dr. Julia Oktawiec (Northwestern University) for helpful discussions and assistance with PXRD data.

REFERENCES

- (1) Furukawa, H.; Cordova, K. E.; O'Keeffe, M.; Yaghi, O. M. The Chemistry and Applications of Metal-Organic Frameworks. *Science* **2013**, *341*, 1230444.
- (2) Cavka, J. H.; Jakobsen, S.; Olsbye, U.; Guillou, N.; Lamberti, C.; Bordiga, S.; Lillerud, K. P. A New Zirconium Inorganic Building Brick Forming Metal Organic Frameworks with Exceptional Stability. *J. Am. Chem. Soc.* **2008**, *130*, 13850–13851.
- (3) Bai, Y.; Dou, Y.; Xie, L.-H.; Rutledge, W.; Li, J.-R.; Zhou, H.-C. Zr-Based Metal—Organic Frameworks: Design, Synthesis, Structure, and Applications. *Chem. Soc. Rev.* **2016**, *45*, 2327—2367.
- (4) Wang, Z.; Bilegsaikhan, A.; Jerozal, R. T.; Pitt, T. A.; Milner, P. J. Evaluating the Robustness of Metal-Organic Frameworks for Synthetic Chemistry. ACS Appl. Mater. Interfaces 2021, 13, 17517–17531.
- (5) Yuan, S.; Qin, J.-S.; Lollar, C. T.; Zhou, H.-C. Stable Metal-Organic Frameworks with Group 4 Metals: Current Status and Trends. ACS Cent. Sci. 2018, 4, 440–450.
- (6) Forgan, R. S. Modulated Self-Assembly of Metal—Organic Frameworks. *Chem. Sci.* **2020**, *11*, 4546—4562.
- (7) Winarta, J.; Shan, B.; Mcintyre, S. M.; Ye, L.; Wang, C.; Liu, J.; Mu, B. A Decade of UiO-66 Research: A Historic Review of Dynamic Structure, Synthesis Mechanisms, and Characterization Techniques of an Archetypal Metal—Organic Framework. *Cryst. Growth Des.* **2020**, 20, 1347—1362.
- (8) Feng, L.; Wang, K.-Y.; Powell, J.; Zhou, H.-C. Controllable Synthesis of Metal-Organic Frameworks and Their Hierarchical Assemblies. *Matter* **2019**, *1*, 801–824.
- (9) Liu, B.; Vellingiri, K.; Jo, S.-H.; Kumar, P.; Ok, Y. S.; Kim, K.-H. Recent Advances in Controlled Modification of the Size and Morphology of Metal-Organic Frameworks. *Nano Res.* **2018**, *11*, 4441–4467.
- (10) Schaate, A.; Roy, P.; Godt, A.; Lippke, J.; Waltz, F.; Wiebcke, M.; Behrens, P. Modulated Synthesis of Zr-Based Metal-Organic Frameworks: From Nano to Single Crystals. *Chem. Eur. J.* **2011**, *17*, 6643–6651.
- (11) Wu, H.; Chua, Y. S.; Krungleviciute, V.; Tyagi, M.; Chen, P.; Yildirim, T.; Zhou, W. Unusual and Highly Tunable Missing-Linker Defects in Zirconium Metal—Organic Framework UiO-66 and Their Important Effects on Gas Adsorption. *J. Am. Chem. Soc.* **2013**, *135*, 10525—10532.

- (12) Shan, B.; McIntyre, S. M.; Armstrong, M. R.; Shen, Y.; Mu, B. Investigation of Missing-Cluster Defects in UiO-66 and Ferrocene Deposition into Defect-Induced Cavities. *Ind. Eng. Chem. Res.* **2018**, 57, 14233–14241.
- (13) Zahn, G.; Zerner, P.; Lippke, J.; Kempf, F. L.; Lilienthal, S.; Schröder, C. A.; Schneider, A. M.; Behrens, P. Insight into the Mechanism of Modulated Syntheses: *In Situ Synchrotron Diffraction Studies on the Formation of Zr-Fumarate MOF. CrystEngComm* **2014**, *16*, 9198–9207.
- (14) Gu, Y.; Xie, D.; Ma, Y.; Qin, W.; Zhang, H.; Wang, G.; Zhang, Y.; Zhao, H. Size Modulation of Zirconium-Based Metal Organic Frameworks for Highly Efficient Phosphate Remediation. ACS Appl. Mater. Interfaces 2017, 9, 32151–32160.
- (15) Shearer, G. C.; Chavan, S.; Bordiga, S.; Svelle, S.; Olsbye, U.; Lillerud, K. P. Defect Engineering: Tuning the Porosity and Composition of the Metal—Organic Framework UiO-66 via Modulated Synthesis. *Chem. Mater.* **2016**, 28, 3749—3761.
- (16) Ren, J.; Langmi, H. W.; North, B. C.; Mathe, M.; Bessarabov, D. Modulated Synthesis of Zirconium-Metal Organic Framework (Zr-MOF) for Hydrogen Storage Applications. *Int. J. Hydrogen Energy* **2014**, *39*, 890–895.
- (17) Gutov, O. V.; Hevia, M. G.; Escudero-Adán, E. C.; Shafir, A. Metal—Organic Framework (MOF) Defects under Control: Insights into the Missing Linker Sites and Their Implication in the Reactivity of Zirconium-Based Frameworks. *Inorg. Chem.* **2015**, *54*, 8396–8400.
- (18) Morris, W.; Wang, S.; Cho, D.; Auyeung, E.; Li, P.; Farha, O. K.; Mirkin, C. A. Role of Modulators in Controlling the Colloidal Stability and Polydispersity of the UiO-66 Metal—Organic Framework. ACS Appl. Mater. Interfaces 2017, 9, 33413—33418.
- (19) Hu, Z.; Peng, Y.; Kang, Z.; Qian, Y.; Zhao, D. A Modulated Hydrothermal (MHT) Approach for the Facile Synthesis of UiO-66-Type MOFs. *Inorg. Chem.* **2015**, *54*, 4862–4868.
- (20) Katz, M. J.; Brown, Z. J.; Colón, Y. J.; Siu, P. W.; Scheidt, K. A.; Snurr, R. Q.; Hupp, J. T.; Farha, O. K. A Facile Synthesis of UiO-66, UiO-67 and Their Derivatives. *Chem. Commun.* **2013**, 49, 9449.
- (21) Vermoortele, F.; Bueken, B.; Le Bars, G.; Van de Voorde, B.; Vandichel, M.; Houthoofd, K.; Vimont, A.; Daturi, M.; Waroquier, M.; Van Speybroeck, V.; Kirschhock, C.; De Vos, D. E. Synthesis Modulation as a Tool To Increase the Catalytic Activity of Metal—Organic Frameworks: The Unique Case of UiO-66(Zr). *J. Am. Chem. Soc.* 2013, 135, 11465–11468.
- (22) Ragon, F.; Horcajada, P.; Chevreau, H.; Hwang, Y. K.; Lee, U.-H.; Miller, S. R.; Devic, T.; Chang, J.-S.; Serre, C. In Situ Energy-Dispersive X-Ray Diffraction for the Synthesis Optimization and Scale-up of the Porous Zirconium Terephthalate UiO-66. *Inorg. Chem.* **2014**, *53*, 2491–2500.
- (23) Han, Y.; Liu, M.; Li, K.; Zuo, Y.; Wei, Y.; Xu, S.; Zhang, G.; Song, C.; Zhang, Z.; Guo, X. Facile Synthesis of Morphology and Size-Controlled Zirconium Metal—Organic Framework UiO-66: The Role of Hydrofluoric Acid in Crystallization. *CrystEngComm* **2015**, 17, 6434—6440.
- (24) Marshall, R. J.; Hobday, C. L.; Murphie, C. F.; Griffin, S. L.; Morrison, C. A.; Moggach, S. A.; Forgan, R. S. Amino Acids as Highly Efficient Modulators for Single Crystals of Zirconium and Hafnium Metal—Organic Frameworks. *J. Mater. Chem. A* **2016**, *4*, 6955—6963.
- (25) Gutov, O. V.; Molina, S.; Escudero-Adán, E. C.; Shafir, A. Modulation by Amino Acids: Toward Superior Control in the Synthesis of Zirconium Metal-Organic Frameworks. *Chem. Eur. J.* **2016**, *22*, 13582–13587.
- (26) Atzori, C.; Shearer, G. C.; Maschio, L.; Civalleri, B.; Bonino, F.; Lamberti, C.; Svelle, S.; Lillerud, K. P.; Bordiga, S. Effect of Benzoic Acid as a Modulator in the Structure of UiO-66: An Experimental and Computational Study. *J. Phys. Chem. C* **2017**, *121*, 9312–9324.
- (27) Rubio-Martinez, M.; Avci-Camur, C.; Thornton, A. W.; Imaz, I.; Maspoch, D.; Hill, M. R. New Synthetic Routes towards MOF Production at Scale. *Chem. Soc. Rev.* **2017**, *46*, 3453–3480.
- (28) Armstrong, M. R.; Arredondo, K. Y. Y.; Liu, C.-Y.; Stevens, J. E.; Mayhob, A.; Shan, B.; Senthilnathan, S.; Balzer, C. J.; Mu, B. UiO-66 MOF and Poly(Vinyl Cinnamate) Nanofiber Composite

- Membranes Synthesized by a Facile Three-Stage Process. *Ind. Eng. Chem. Res.* **2015**, *54*, 12386–12392.
- (29) Nayuk, R.; Zacher, D.; Schweins, R.; Wiktor, C.; Fischer, R. A.; van Tendeloo, G.; Huber, K. Modulated Formation of MOF-5 Nanoparticles—A SANS Analysis. *J. Phys. Chem. C* **2012**, *116*, 6127–6135
- (30) Guo, H.; Zhu, Y.; Wang, S.; Su, S.; Zhou, L.; Zhang, H. Combining Coordination Modulation with Acid–Base Adjustment for the Control over Size of Metal–Organic Frameworks. *Chem. Mater.* **2012**, 24, 444–450.
- (31) Cravillon, J.; Nayuk, R.; Springer, S.; Feldhoff, A.; Huber, K.; Wiebcke, M. Controlling Zeolitic Imidazolate Framework Nano- and Microcrystal Formation: Insight into Crystal Growth by Time-Resolved In Situ Static Light Scattering. *Chem. Mater.* **2011**, 23, 2130–2141.
- (32) Diring, S.; Furukawa, S.; Takashima, Y.; Tsuruoka, T.; Kitagawa, S. Controlled Multiscale Synthesis of Porous Coordination Polymer in Nano/Micro Regimes. *Chem. Mater.* **2010**, *22*, 4531–4538.
- (33) Hermes, S.; Witte, T.; Hikov, T.; Zacher, D.; Bahnmüller, S.; Langstein, G.; Huber, K.; Fischer, R. A. Trapping Metal-Organic Framework Nanocrystals: An *in-Situ* Time-Resolved Light Scattering Study on the Crystal Growth of MOF-5 in Solution. *J. Am. Chem. Soc.* **2007**, *129*, 5324–5325.
- (34) Griffin, S. L.; Briuglia, M. L.; ter Horst, J. H.; Forgan, R. S. Assessing Crystallisation Kinetics of Zr Metal—Organic Frameworks through Turbidity Measurements to Inform Rapid Microwave-Assisted Synthesis. *Chem. Eur. J.* **2020**, *26*, 6910–6918.
- (35) Le Bail, A. Whole Powder Pattern Decomposition Methods and Applications: A Retrospection. *Powder Diffr.* **2005**, *20*, 316–326.
- (36) Ejegbavwo, O. A.; Martin, C. R.; Olorunfemi, O. A.; Leith, G. A.; Ly, R. T.; Rice, A. M.; Dolgopolova, E. A.; Smith, M. D.; Karakalos, S. G.; Birkner, N.; Powell, B. A.; Pandey, S.; Koch, R. J.; Misture, S. T.; Loye, H.-C. z.; Phillpot, S. R.; Brinkman, K. S.; Shustova, N. B. Thermodynamics and Electronic Properties of Heterometallic Multinuclear Actinide-Containing Metal—Organic Frameworks with "Structural Memory". J. Am. Chem. Soc. 2019, 141, 11628–11640.
- (37) Diffraction Analysis of the Microstructure of Materials; Mittemeijer, E. J.; Scardi, P., Eds.; Hull, R.; Osgood, R. M.; Parisi, J.; Warlimont, H., Series Eds.; Springer Series in Materials Science; Springer Berlin Heidelberg: Berlin, Heidelberg, 2004; Vol. 68, DOI: 10.1007/978-3-662-06723-9.
- (38) Cliffe, M. J.; Wan, W.; Zou, X.; Chater, P. A.; Kleppe, A. K.; Tucker, M. G.; Wilhelm, H.; Funnell, N. P.; Coudert, F.-X.; Goodwin, A. L. Correlated Defect Nanoregions in a Metal—Organic Framework. *Nat. Commun.* **2014**, *5*, 4176.
- (39) Mondloch, J. E.; Bury, W.; Fairen-Jimenez, D.; Kwon, S.; DeMarco, E. J.; Weston, M. H.; Sarjeant, A. A.; Nguyen, S. T.; Stair, P. C.; Snurr, R. Q.; Farha, O. K.; Hupp, J. T. Vapor-Phase Metalation by Atomic Layer Deposition in a Metal—Organic Framework. *J. Am. Chem. Soc.* **2013**, *135*, 10294—10297.
- (40) Kickelbick, G.; Wiede, P.; Schubert, U. Variations in Capping the $Zr_6O_4(OH)_4$ Cluster Core: X-Ray Structure Analyses of $[Zr_6(OH)_4O_4(OOC-CH=CH_2)_{10}]_2(\mu\text{-OOC}-CH=CH_2)_4$ and $Zr_6(OH)_4O_4(OOCR)_{12}(PrOH)$ (R = Ph, CMe = CH₂). *Inorg. Chim. Acta* 1999, 284, 1–7.
- (41) Webber, T. E.; Liu, W.-G.; Desai, S. P.; Lu, C. C.; Truhlar, D. G.; Penn, R. L. Role of a Modulator in the Synthesis of Phase-Pure NU-1000. ACS Appl. Mater. Interfaces 2017, 9, 39342–39346.
- (42) Liljefors, T.; Krogsgaard-Larsen, P.; Madsen, U. Textbook of Drug Design and Discovery, Third Edition; Forensic Science; Taylor & Francis: 2002.
- (43) Hansch, C. H.; Leo, A. Substituent Constants for Correlation Analysis in Chemistry and Biology; John Wiley & Sons: New York, 1979
- (44) Belot, V.; Farran, D.; Jean, M.; Albalat, M.; Vanthuyne, N.; Roussel, C. Steric Scale of Common Substituents from Rotational

- Barriers of N-(o-Substituted aryl)thiazoline-2-thione Atropisomers. J. Org. Chem. 2017, 82, 10188–10200.
- (45) Saethre, L. J.; Thomas, T. D. Relationships between Electronic Substituent Parameters. J. Phys. Org. Chem. 1991, 4, 629–634.
- (46) Sakloth, F.; Kolanos, R.; Mosier, P. D.; Bonano, J. S.; Banks, M. L.; Partilla, J. S.; Baumann, M. H.; Negus, S. S.; Glennon, R. A. Steric Parameters, Molecular Modeling and Hydropathic Interaction Analysis of the Pharmacology of Para-Substituted Methcathinone Analogues: Further QSAR of Para-Substituted Methcathinone Analogues. Br. J. Pharmacol. 2015, 172, 2210–2218.
- (47) Øien, S.; Wragg, D.; Reinsch, H.; Svelle, S.; Bordiga, S.; Lamberti, C.; Lillerud, K. P. Detailed Structure Analysis of Atomic Positions and Defects in Zirconium Metal—Organic Frameworks. *Cryst. Growth Des.* **2014**, *14*, 5370—5372.
- (48) Yamashita, M.; Hartwig, J. F. Synthesis, Structure, and Reductive Elimination Chemistry of Three-Coordinate Arylpalladium Amido Complexes. *J. Am. Chem. Soc.* **2004**, *126*, 5344–5345.
- (49) Zeng, Y.; Moghadam, P. Z.; Snurr, R. Q. Pore Size Dependence of Adsorption and Separation of Thiophene/Benzene Mixtures in Zeolites. *J. Phys. Chem. C* **2015**, *119*, 15263–15273.
- (50) Wang, K.; Li, C.; Liang, Y.; Han, T.; Huang, H.; Yang, Q.; Liu, D.; Zhong, C. Rational Construction of Defects in a Metal—Organic Framework for Highly Efficient Adsorption and Separation of Dyes. *Chem. Eng. J.* **2016**, 289, 486–493.
- (51) Li, B.; Zhu, X.; Hu, K.; Li, Y.; Feng, J.; Shi, J.; Gu, J. Defect Creation in Metal-Organic Frameworks for Rapid and Controllable Decontamination of Roxarsone from Aqueous Solution. *J. Hazard. Mater.* **2016**, 302, 57–64.
- (52) Cliffe, M. J.; Hill, J. A.; Murray, C. A.; Coudert, F.-X.; Goodwin, A. L. Defect-Dependent Colossal Negative Thermal Expansion in UiO-66(Hf) Metal—Organic Framework. *Phys. Chem. Chem. Phys.* **2015**, *17*, 11586—11592.
- (53) Van de Voorde, B.; Stassen, I.; Bueken, B.; Vermoortele, F.; De Vos, D.; Ameloot, R.; Tan, J.-C.; Bennett, T. D. Improving the Mechanical Stability of Zirconium-Based Metal—Organic Frameworks by Incorporation of Acidic Modulators. *J. Mater. Chem. A* **2015**, 3, 1737–1742.
- (54) Shearer, G. C.; Chavan, S.; Ethiraj, J.; Vitillo, J. G.; Svelle, S.; Olsbye, U.; Lamberti, C.; Bordiga, S.; Lillerud, K. P. Tuned to Perfection: Ironing Out the Defects in Metal—Organic Framework UiO-66. Chem. Mater. 2014, 26, 4068—4071.
- (55) Valenzano, L.; Civalleri, B.; Chavan, S.; Bordiga, S.; Nilsen, M. H.; Jakobsen, S.; Lillerud, K. P.; Lamberti, C. Disclosing the Complex Structure of UiO-66 Metal Organic Framework: A Synergic Combination of Experiment and Theory. *Chem. Mater.* **2011**, *23*, 1700–1718.
- (56) Shearer, G. C.; Vitillo, J. G.; Bordiga, S.; Svelle, S.; Olsbye, U.; Lillerud, K. P. Functionalizing the Defects: Postsynthetic Ligand Exchange in the Metal Organic Framework UiO-66. *Chem. Mater.* **2016**, *28*, 7190–7193.
- (57) Jiang, H.-L.; Feng, D.; Liu, T.-F.; Li, J.-R.; Zhou, H.-C. Pore Surface Engineering with Controlled Loadings of Functional Groups via Click Chemistry in Highly Stable Metal—Organic Frameworks. *J. Am. Chem. Soc.* **2012**, *134*, 14690–14693.